DOI: 10.1002/((please add manuscript number))

Article type: Communication

Single-Layer-Particle Electrode Design for Practical Fast-Charging Lithium-ion Batteries

Shuibin Tu, Ziheng Lu, Mengting Zheng, Zihe Chen, Xiancheng Wang, Zhao Cai, Chaoji Chen, Li Wang, Chenhui Li, Zhi Wei Seh, Shangqing Zhang, Jun Lu, and Yongming Sun**

S. B. Tu, Z. H. Chen, X. C. Wang, Dr. Z. Cai, Prof. Y. Sun

Wuhan National Laboratory for Optoelectrons and School of Optical and Electron Information,

Huazhong University of Science and Technology, Wuhan, 430074, China.

E-mail: yongmingsun@hust.edu.cn

Dr. Z. H. Lu

Department of Materials Science and Metallurgy, University of Cambridge, Cambridge, CB3 0FS, United Kingdom.

M. T. Zheng, Prof. S. Q. Zhang

Centre for Clean Environment and Energy, School of Environment and Science, Gold Coast 11 Campus, Griffith University, Gold Coast 4222, Australia.

S. B. Tu, Prof. C. H. Li

Department of Materials Science and Engineering, Huazhong University of Science and Technology, Wuhan, 430074, China.

Prof. C. J. Chen

Hubei Key Laboratory of Biomass Resource Chemistry and Environmental Biotechnology, Hubei International Scientific and Technological Cooperation Base of Sustainable Resource and Energy, Hubei Engineering Center of Natural Polymers-Based Medical Materials, School of Resource and Environmental Science, Wuhan University, Wuhan 430079, China.

Prof. L. Wang

Institute of Nuclear & New Energy Technology, Tsinghua University, Beijing 100084, China.

Prof. Z. W. Seh

Institute of Materials Research and Engineering, Agency for Science, Technology and Research (A*STAR), 2 Fusionopolis Way, Innovis, Singapore 138634, Singapore.

Dr. J. Lu

Chemical Sciences and Engineering Division, Argonne National Laboratory, Lemont, Illinois 60439, United States.

E-mail: junlu@anl.gov

Keywords: single-layer-particle electrode, fast charging, high power density, high energy density, red phosphorus

Abstract

Efforts to enable fast charging and high energy density lithium-ion batteries (LIBs) are hampered by the trade-off nature of the traditional electrode design: increasing the areal capacity usually comes with sacrificing the fast charge transfer. Here we report a single-layer chunky particle electrode design, where red phosphorus active material is embedded in nanochannels of vertically aligned graphene (red P/VAG) assemblies. Such electrode design addresses the sluggish charge transfer stemming from the high tortuosity and inner particle/electrode resistance of traditional electrode architectures consisting of randomly stacked active particles. The vertical ion transport nanochannels and electron transfer conductive nanowalls of graphene confine the direction of charge transfer to minimize the transfer distance, and the incomplete filling of nanochannels in the red P/VAG composite buffers volume change locally, thus avoiding the variation of electrodes thickness during cycling. The single-layer chunky particle electrode displays a high areal capacity (5.6 mAh cm-

^{2}), which was the highest among the reported fast-charging battery chemistries. Paired with a high-loading $LiNi_{0.6}Co_{0.2}Mn_{0.2}O_2$ (NCM622) cathode, a pouch cell showed stable cycling with high energy density (405 Wh kg^{-1}, 1040 Wh L^{-1}), and power density (1224 W kg^{-1} and 3137 W L^{-1} at 6 C, 30 mA cm^{-2}). Such single-layer chunky particle electrode design with inner vertical charge transport pathways can be extended to other advanced battery systems and boost the development of LIBs with fast-charging capability and high energy density.

Introduction

High energy density lithium-ion batteries (LIBs) with fast-charging capability is highly desirable for portable electronics and electric vehicles.[1-6] Considering the limited energy and power density of traditional intercalation-type materials,[7-12] using high-capacity materials such as alloy type of Si, Sn, or P-based anodes,[13-21] holds the promise in reducing the volume and the weight of the electrodes, therefore, boosting the overall battery energy density. Nonetheless, when the areal capacity of electrodes reaches a substantially high-level capacity (e.g.,> 3.5 mAh cm^{-2}), rate capacity is significantly reduced owing to the increasing charge transfer length and resistance in the thicker electrodes.[22-27] Currently, enormous efforts have been devoted to fabricating nanoscale alloy-type materials and/or their composites with conducting species, which shorten the charge transport distance and improve the conductivities at the particle level.[1, 28-31] However, at the electrode level, the fast-charging capability of these nanostructured anodes is still significantly plagued by the sluggish charge transfer, stemming from the random stacking of nanoparticles and low packing density which entails a high tortuosity and large practical thickness (**Figure 1**, left). Therefore, rational electrode design with space-efficient packing using high-capacity electrode materials with fast charge transfer capability is essential to achieve fast charging LIBs with high areal capacity.

The target of the US Advanced Battery Consortium (USABC) is to realize 80% state of charge within 15 minutes based on the cell-level energy density of 550 Wh L^{-1} and 275 Wh kg^{-1}, making it an important reference for fast-charging battery technology.[32] We believe that materials with rapid electrochemical reactivity and electrode structures designed for fast charge transport are two enablers for fast-charging high energy density LIBs. To realize a space-efficient packing, dense stacking of active materials but with certain void space is expected to minimize electrode thickness and withstand the volume changes during the charge/discharge processes. Furthermore, it is highly desirable to confine the charge transport orientation to maximize charge transport kinetics. However, such electrode designs have not been reported for high energy density LIBs with fast-charging capability.

In this study, we proposed that a single-layer chunky particle electrode architecture with vertically aligned charge transport pathways could realize fast charge transport of high-areal-capacity electrodes, enabling fast-charging capability and high energy density of LIBs (Figure 1, right). Such electrode design addresses the inherent problems of high tortuosity and large inner particle/electrode resistance in the Li^+ transport direction of traditional electrode architectures consisting of randomly stacked active particles. As a demonstration, here we report a single-layer-particle electrode for fast-charging, high energy density battery anode, where red phosphorus (red P),[20] a high capacity (2576 mAh g^{-1}) anode, is embedded in the vertically aligned nanochannels of chunky graphene assemblies (red P/VAG) with fast charge transfer capability. As a result, we have achieved the single-layer red P/VAG particle electrode with a high areal capacity of 5.6 mAh cm^{-2}. When coupled with a high-loading $LiNi_{0.6}Co_{0.2}Mn_{0.2}O_2$ (NCM622) cathode, a pouch cell showed stable cycling with high energy density (405 Wh kg^{-1}, 1040 Wh L^{-1}), and power density (1224 W kg^{-1} and 3137 W L^{-1} at 6 *C*, 30 mA cm^{-2}). The demonstrated strategy starts with tens of microns particle combining vertical charge transport pathways, which is able to balance fast-charging capability and high energy density, and thus represents a promising solution toward practical fast-charging LIBs.

Results and discussion

Fabrication and characterization of single-layer chunky particle electrode

Before the fabrication of the single-layer chunky red P/VAG particle electrode, chunky VAG particles in tens of microns were first synthesized, which consisted of aligned graphene nanosheets with vertical nanochannels. As illustrated in **Figure 2**a, graphene oxide (GO) was used as the framework element, silica (SiO_2) was used as the channel template, and polyaniline (PANI) was served as the adhesive of the VAG. Chunky VAG particles with vertically aligned inner nanochannels were obtained after the co-assembly process, followed by thermal annealing and etching of SiO_2 (the mechanism of VAG formation is described in the Method Section). As revealed by scanning electron microscopy (SEM) images, the size of VAG particles was several tens of microns (Figure 2b). They consisted of aligned graphene nanosheets connected by carbon derived from PANI and possessed parallel nanochannels between the graphene nanosheets with a width of ~ 22 nm (Figure S2). The transmission electron microscopy (TEM) results further verified the well-ordered layer-by-layer structure with parallel nanochannels for VAG (Figure 2c). Such a graphene framework provides continuous conductive pathways for electron transport, low-tortuosity nanochannels for Li^+

diffusion, and abundant space for hosting active red P for rapid electrode electrochemical reactions. Another advantage of the VAG architecture is its high volumetric packing density due to its large overall particle size, which was beneficial for realizing high volumetric capacity. The results of the X-ray photoelectron spectroscopy (XPS) survey spectrum revealed the existence of C, N, and O elements in the VAG, with an atomic percentage of 89.5 %, 6.0 %, and 4.5 %, respectively (Figure S3). The N and O elements were originated from the initial PANI and GO, respectively, and these heteroatoms with high content could form chemical bonds to stabilize active red P.[33]

Red P was incorporated into the VAG *via* a co-evaporation and condensation strategy.[20] Figure 2d displayed the scanning transmission electron microscopy (STEM) and the corresponding energy-dispersive X-ray (EDX) spectroscopy elemental mapping images of the red P/VAG composite. The results verified the homogeneous distribution of C, N, O, and P elements in the tested region of the sample, indicating the uniform implantation of red P into the VAG particles. The N_2 adsorption/desorption isotherm of the VAG and red P/VAG composite displayed typical type-IV isotherms with a distinct hysteresis loop where the relative pressure was above 0.4 (Figure 2e), suggesting its mesoporous structure. The Brunauer-Emmett-Teller (BET) surface area of VAG was 373.9 m^2 g^{-1}, and its pore volume was 2.42 cm^3 g^{-1}, with an average Barrett-Joyner-Halenda (BJH) pore size of 22 nm. The high porosity of the VAG allowed a high red P loading of ~ 85 wt%, which enables the high overall capacity of the red P/VAG composite. After red P implantation, the specific surface area and pore volume of red P/VAG were reduced to 69.6 m^2 g^{-1} and 0.53 cm^3 g^{-1}, respectively, indicating that the nanochannels in the VAG were not completely filled or blocked by red P. The remnant space could act as the pathway for Li$^+$ transport and buffer the volume expansion of red P during the charging/discharging processes.

The single-layer red P/VGA particle electrode was prepared through a traditional doctor blading process, including slurry mixing and coating, and electrode baking and calendaring operations. Two key parameters to ensure the formation of single-layer particle electrode were the slurry concentration and the distance between the blade and current collector for slurry coating (Figure S10). SEM images showed single-layer particle structure of the red P/VAG particle electrode with a thickness of ~ 60 μm (Figure 2f). During the slurry coating process, the red P/VAG particles tended to lie down with the inner graphene layers and nanochannels perpendicular to the Cu current collector due to their analogy rectangle geometry, forming a low-tortuosity pore structure of the electrode for fast ion transfer and a vertical conductive pathway for rapid electron transport (Figure 2g). Such an electrode architecture is intrinsically different from the reported three-dimension (3D) electrodes with large pore size (10–200 μm) and high porosity, which lead to low practical overall capacity and energy density in consideration of the entire mass of materials and electrolyte intake (e.g., graphene sponge, 3D aligned graphene array, and carbonized wood, etc).[34-38] The unique geometry and large size of red P/VAG composite enabled single-layer-particle electrode with high packing density (0.9 g cm^{-3}) and high active materials loading (4.2 mg cm^{-2} for 60 μm-thick electrode), making it feasible to achieve high areal capacity and high volumetric capacity. Meanwhile, the single-layer-particle electrode could eliminate the interparticle resistance in the direction of Li^{+} and electron transport. Thus, it is expected to achieve high rate capability at high areal capacity conditions. Furthermore, the robust graphene array architecture could endow the red P/VAG electrode with excellent mechanical stability and effectively relieve the strain during cycling.

Electrochemical evaluation of single-layer chunky particle electrode

To demonstrate the superiority of single-layer red P/VAG particle electrode for fast-charging batteries, its electrochemical lithium storage property was first investigated in a half cell configuration with Li metal foil as the counter electrode in the potential range of 0.01–2.0 V. The capacity-cycle number plots and the corresponding voltage-capacity plots under various current densities from 1 to 8 mA cm^{-2} were shown in Figure S12. After 4 activation cycles at 0.5 mA cm^{-2}, the single-layer red P/VAG particle electrode displayed a high overall charge specific capacity of 1011 mAh g^{-1} and an areal capacity of 5.6 mAh cm^{-2} at 1 mA cm^{-2}, much higher than that of the commercial anodes (e.g., ~3.5 mAh cm^{-2} for graphite). Even at a high current density of 8 mA cm^{-2}, it still exhibited a high areal capacity of 4.0 mAh cm^{-2} with a high-capacity retention rate of 71.4%. The superior fast-charging capability of the single-layer red P/VAG particle electrode could be attributed to its low interparticle resistance, low pore tortuosity, and excellent electrical conductivity. To demonstrate the significant superiorities of the single-layer red P/VAG particle electrode for high energy density and fast-charging batteries, electrodes of the single-layer red P/VAG, commercial $Li_4Ti_5O_{12}$ and graphite were compared with the same areal capacity of ~ 5.6 mAh cm^{-2} at 1 mA cm^{-2}. As shown in **Figure 3**a-c, the thicknesses of the three electrodes were 60, 156, and 257 μm, respectively. The small thickness of the single-layer red P/VAG electrode afforded a high volumetric capacity of 933 mAh cm^{-3}, which was much higher than that of graphite and $Li_4Ti_5O_{12}$ electrodes (359 and 218 mAh cm^{-3}, respectively). Moreover, the single-layer red P/VAG particle electrode also delivered the highest specific capacity of 1077 mAh g^{-1} among the three electrodes, about four times and six times higher than that of the graphite electrode (256 mAh g^{-1}) and $Li_4Ti_5O_{12}$ electrode (157 mAh g^{-1}), respectively. Furthermore, the rate capabilities of graphite and $Li_4Ti_5O_{12}$ electrodes were also measured at the same conditions with the single-layer red P/VAG particle electrode (Figure S15). The capacity retentions for graphite and $Li_4Ti_5O_{12}$ electrodes were 7% and 27.3% at 8 mA cm^{-2}, respectively, much lower than the 71.4% for the single-layer red P/VAG particle electrode. More impressively, the fast-charging capability of single-layer red P/VAG particle electrode at high areal capacity conditions exceeded those of the reported advanced electrodes constructed by phosphorus, silicon and other high-rate materials (Figure 3d and Table S1).

Cyclic voltammetry (CV) measurements, galvanostatic intermittent titration technique (GITT), and electrochemical impedance spectroscopy (EIS) were employed to investigate the diffusion behaviors and interfacial kinetic properties of single-layer red P/VAG particle electrode. The CV curves at the scanning rates from 0.03 to 0.1 mV s^{-1} (Figure S17) were recorded, and diffusion-controlled kinetics for the single-layer red P/VAG particle electrode was evaluated according to the relationship between square root scan rates and peaks, which highlighted the importance of the regulation of charge transport in electrodes for fast charging. The calculated Li^+ diffusion coefficients (D_{Li+}) based on two cathodic peaks for lithiation were 4.8×10^{-8} and 1.6×10^{-8} cm^{-2} s^{-1}, respectively, which was lower than 6.0×10^{-8} cm^{-2} s^{-1} for delithiation. These results suggested the slower lithiation reaction kinetics than the delithiation reaction kinetics, making fast charging more challenging than fast discharging. Moreover, the D_{Li+} value based on GITT (Figure S18) for the single-layer red P/VAG particle electrode was much higher than the reported P-based electrodes, which was attributed to the low tortuosity and vertical nanochannel structure of the single-layer red P/VAG particle electrode. The EIS spectra (Figure S19 and S20) of the single-layer red P/VAG particle electrode showed low interfacial resistance and charge transfer resistance, and remained almost constant after 70 cycles, again suggesting its fast charge transport capability and stable structure on cycling.

The electrochemical cycling stability of the single-layer red P/VAG particle electrode was further studied. It delivered an areal capacity of 5.6 mAh cm^{-2} at 1 mA cm^{-2} after two activation cycles and the capacity retention was 71.4% for 140 cycles with the average Coulombic efficiency as high as 99.5%, indicating high reversibility of the single-layer red P/VAG particle electrode (Figure S21 and S23). Note that higher areal capacity loading could be easily realized by fabricating double-layer red P/VAG electrode. A double-layer red P/VAG electrode with mass loading of ~8.4 mg cm^{-2} showed an ultrahigh areal capacity of 9.8 mAh cm^{-2} at 1 mA cm^{-2} with the specific capacity of 933.3 mAh g^{-1} based on the total mass of the red P/VAG electrode, as well as stable cycling performance (Figure S25 and S26). The specific capacity of the double-layer red P/VAG particle electrode was slightly lower than that of the single-layer particle electrode due to the increased electrode thickness and the reduced utilization ratio of active materials. Till now, few reports showed the satisfactory electrochemical results of electrodes consisting of alloy-type materials with a high capacity > 5 mAh cm^{-2} using traditional slurry-coated electrodes due to the large accumulated volume strains. These results indicated the superior structural advantages of red P/VAG architecture in realizing high-areal-capacity electrodes with long cycle life in comparison to other alloy-type anodes (Figure S27 and Table S2).

To reveal the effect of electrode structure on fast charging, we simulated the electrode-level Li^+ transport and electrode overpotentials in regular particle and single-layer-particle electrodes (Figure 3e and 3f). For the single-layer-particle electrode, ions can transport rapidly from one end to the opposite in a straight path, resulting in a lower concentration gradient of Li^+ in the electrode. In particular, the concentration of Li^+ at the vertical depth of 50 μm is ~88% of the bulk electrolyte concentration (Figure 3g). In sharp contrast, in regular particle electrodes with numerous randomly stacked particles, Li^+ has to travel extended distances along the highly convoluted pathways, resulting in an obvious Li^+ concentration gradient even at a small vertical depth of 200 nm and the Li^+ concentration at the electrode depth of 50 μm is only ~54% of that at the electrode top. Therefore, slow Li^+ transport within the traditional porous electrode becomes one of the limiting factors for fast charging, which would cause the lack of lithium supply within the electrode for fast electrochemical reaction. In addition, for regular particle electrode, overpotentials build up unevenly and increase significantly from the top to the bottom of the electrode due to large interparticle resistance (Figure 3h), which also contributes to the poor rate capability. While for the single-layer-particle electrode, the overpotentials with a smaller value are built up uniformly since the single-layer active particle architecture could eliminate the interparticle resistance in the direction of Li^+ transport. The finite element simulation results indicate that our proposed single-layer-particle electrode is a promising electrode architecture for fast-charging LIBs owing to its superiority in promoting Li^+ transport, reducing and homogenizing electrode overpotentials over conventional particle electrodes.

To further investigate the fast-charging capability of single-layer red P/VAG particle electrode in high-energy-density LIBs, high mass loading $LiNi_{0.6}Co_{0.2}Mn_{0.2}O_2$ (NCM622) or $LiCoO_2$ (LCO) cathodes were fabricated (Figure S28). The NCM622||single-layer red P/VAG full cell delivered a high areal capacity of 5.4 mAh cm^{-2} at 1 mA cm^{-2} and displayed outstanding fast charging capability with areal capacities of 4.9, 4.3, 3.6, 3.1, 2.8, 2.6, and 2.2 mAh cm^{-2}

in 60, 30, 20, 15, 12, 10, and 8 min charging times, corresponding to charging current densities of 5, 10, 15, 20, 25, 30, and 40 mA cm^{-2}, respectively (**Figure 4**a and 4b). Moreover, LCO||single-layer red P/VAG full cell also exhibited excellent fast charging capability (Figure S30 and S31). The cycling stability of NCM622||single-layer red P/VAG and LCO||single-layer red P/VAG full cells under deep lithiation and fast charging conditions were also investigated. The NCM622||single-layer red P/VAG full cell with cathode mass loading of 26.6 mg cm^{-2} exhibited a high areal capacity of 5 mAh cm^{-2} at 1 mA cm^{-2} with a capacity retention of 96% for 180 cycles (Figure S32a). As shown in Figure S32b, the NCM622||single-layer red P/VAG full cell showed stable Coulombic efficiency on cycling with a high average Coulombic efficiency of 99.9%. Figure S32c exhibited the typical charging/discharging voltage profiles of the NCM622||single-layer red P/VAG cells for different cycles, which showed highly overlapped curves with a stable discharge platform at around 2.7 V. More impressively, both the NCM622||single-layer red P/VAG and LCO||single-layer red P/VAG full cells displayed excellent cycling stability under repeated fast charging operations. The NCM622||single-layer red P/VAG cell delivered areal capacities of 3.1 and 2.6 mAh cm^{-2} even at ultrahigh charging current densities of 20 and 30 mA cm^{-2}, corresponding to the charging times of 15 and 10 min, respectively, and the capacity retentions for cycling at 20 and 30 mA cm^{-2} were 80.6% and 76.9% for 350 cycles (Figure 4c and Figure S33), respectively. The LCO||single-layer red P/VAG full cell also delivered a high areal capacity of 2.6 mAh cm^{-2} at 30 mA cm^{-2} with a capacity retention rate of 70% after 450 cycles (Figure 4d and Figure S34). In brief, full cells using the single-layer red P/VAG particle electrode delivered high areal capacity, superior fast charging capability, and stable cycling performance, simultaneously. These results demonstrated the advancement of our single-layer red P/VAG particle electrode configuration in simultaneously realizing high energy density, fast charging, and long lifespan of LIBs. The excellent electrochemical performance was attributed to the unique single-layer red P/VAG particle electrode configuration, which eliminated the interparticle resistance in the direction of Li^+ transport, provided low-tortuosity Li^+ nanochannels and high electron conductivity networks, and homogenized the electrochemical reactions. To further verify the good stability of the single-layer red P/VAG particle electrode, the morphology and composition of the cycled electrodes after 300 cycles at 30 mA cm^{-2} were investigated by SEM (Figure S35). The single-layer red P/VAG particle electrode maintained its morphology and structure. Its thickness was ~70 μm after 300 cycles, with a 16.7% increase in comparison to ~ 60 μm for the initial electrode before cycling. No cracks were observed for the red P/VAG particles. They were in good contact with each other on the Cu foil current collector. These results suggested the good stability of the red P/VAG both at particle and electrode levels, which supported the stable cycling performance under fast charging conditions.

Demonstration of fast-charging full pouch cell

To further demonstrate the viability of single-layer red P/VAG particle electrodes in high-performance LIBs, a pouch-type full cell consisting of NCM622 cathode and single-layer red P/VAG anode was fabricated and measured in the potential range of 1.5–3.8 V (**Figure 5**a). The energy density of the cell reached as high as 405 Wh kg^{-1} and 1040 Wh L^{-1} (tested at a current density of 1 mA cm^{-2}). Impressively, high energy densities of 346 Wh kg^{-1} (887 Wh L^{-1}), 255 Wh kg^{-1} (654 Wh L^{-1}), and 204 Wh kg^{-1} (523 Wh L^{-1}), and high-power densities of 692 W kg^{-1} (1775 W L^{-1}), 1017 W kg^{-1} (2608 W L^{-1}), and 1224 W kg^{-1} (3137 W L^{-1}) were achieved with 30, 15, and 10 min charging times, corresponding to charging current densities of 10, 20, 25 and 30 mA cm^{-2}, respectively (Figure 5 b-d and Table S3). Note that the volumetric energy density for 15 min charging (654 Wh L^{-1}) was far beyond the goal of USABC for fast charging (80% of 550 Wh L^{-1}).[32] These results indicated the practical LIBs with simultaneous high energy density and power density were realized using the single-layer red P/VAG particle electrode configuration. The Ragone plots in Figure 5e revealed that the energy and power densities of NCM622||single-layer red P/VAG pouch-type cell were among the best electrochemical storage systems. The cycling performance of NCM622||single-layer red P/VAG pouch-type full cell under fast charging conditions was also investigated (Figure 5f and 5g). It delivered an energy density of 308 Wh kg^{-1} and 792 Wh l^{-1} in 20 min, and 76.6% energy density can be maintained after 300 cycles, demonstrating its good electrochemical cycling stability under fast charging conditions.

Conclusions

In summary, a single-layer chunky particle electrode consisting of red P filled in vertically aligned graphene assemblies with vertical charge transport pathways was designed and fabricated, which enabled fast-charging, high-energy-density LIBs. As expected, the single-layer red P/VAG particle electrode showed superior cycling stability and fast charging capability in both half-cell and full-cell configurations under high areal capacity (5.6 mAh cm^{-2}). The practical application of the single-layer red P/VAG particle electrode was demonstrated in pouch cells by pairing high-loading NCM622 cathodes, which displayed high energy and power densities, as well as stable cycling stability. The cell delivered high gravimetric energy densities of 405 Wh kg^{-1} and 1040 Wh L^{-1}, and high power densities of 1224 W kg^{-1} and 3137 W L^{-1} at 6 *C*, 30 mA cm^{-2}. The presented single-layered P/VAG particle electrode configuration addressed the main challenge of slow charge transport in traditional porous particle electrodes with high areal capacities. We believe that such electrode design can be extended to other advanced electrode systems and boost the development of LIBs with both fast-charging capability and high energy densities.

References

[1] Y. M. Sun, N. Liu, Y. Cui, *Nat. Energy* **2016**, *1*, 16071.

[2] K. Kang, Y. S. Meng, J. Breger, C. P. Grey, G. Ceder, *Science* **2006**, *311*, 977.

[3] J.-N. Zhang, Q. H. Li, C. Y. Ouyang, X. Q. Yu, M. Y. Ge, X. J. Huang, E. Y. Hu, C. Ma, S. F. Li, R. J. Xiao, W. L. Yang, Y. Chu, Y. J. Liu, H. G. Yu, X.-Q. Yang, X. J. Yang, L. Q. Chen, H. Li, *Nat. Energy* **2019**, *4*, 594.

[4] W. L. Cai, Y.-X. Yao, G.-L. Zhu, C. Yan, L.-L. Jiang, C. X. He, J.-Q. Huang, Q. Zhang, *Chem. Soc. Rev.* **2020**, *49*, 3806.

[5] S. S. Zhang, *ChemElectroChem* **2020**, *7*, 3569.

[6] Q. Ni, L. M. Zheng, Y. Bai, T. C. Liu, H. X. Ren, H. J. Xu, C. Wu, J. Lu, *ACS Energy Lett.* **2020**, *5*, 1763.

[7] W. L. Cai, C. Yan, Y.-X. Yao, L. Xu, R. Xu, L.-L. Jiang, J.-Q. Huang, Q. Zhang, *Small Struct.* **2020**, *1*, 2000010.

[8] W. Zhang, D.-H. Seo, T. Chen, L. J. Wu, M. Topsakal, Y. M. Zhu, D. Y. Lu, G. Ceder, F. Wang, *Science* **2020**, *367*, 1030.

[9] S. T. Fu, X. F. Yu, Q. L. Wu, X. F. Yang, Z. Liu, X. H. Li, S. M. He, D. Wang, Y. C. Li, S. F. Tong, M. M. Wu, *Adv. Energy Mater.* **2021**, *11*, 2003270.

[10] K. J. Griffith, K. M. Wiaderek, G. Cibin, L. E. Marbella, C. P. Grey, *Nature* **2018**, *559*, 556.

[11] H. D. Liu, Z. Y. Zhu, Q. Z. Yan, S. C. Yu, X. He, Y. Chen, R. Zhang, L. Ma, T. C. Liu, M. Li, R. Q. Lin, Y. M. Chen, Y. J. Li, X. Xing, Y. J. Choi, L. Gao, H. S. Cho, K. An, J. Feng, R. Kostecki, K. Amine, T. P. Wu, J. Lu, H. L. Xin, S. P. Ong, P. Liu, *Nature* **2020**, *585*, 63.

[12] T. Tian, L.-L. Lu, Y.-C. Yin, F. Li, T.-W. Zhang, Y.-H. Song, Y.-H. Tan, H.-B. Yao, *Adv. Funct. Mater*. **2021**, *31*, 2007419.

[13] C. Z. Zhang, F. Wang, J. Han, S. Bai, J. Tan, J. S. Liu, F. Li, *Small Struct.* **2021**, *2*, 2100009.

[14] M. Ko, S. Chae, J. Ma, N. Kim, H.-W. Lee, Y. Cui, J. Cho, *Nat. Energy* **2016**, *1*, 16113.

[15] Z. Dong, W. B. Du, H. T. Gu, Y. Y. Long, C. Y. Zhang, G. R. Chen, Z. H. Feng, W. P. Sun, Y. Z. Jiang, Y. F. Liu, Y. X. Yang, J. T. Gan, M. X. Gao, H. G. Pan, *Small Struct.* **2022**, *3*, 2100174.

[16] N. Kim, S. Chae, J. Ma, M. Ko, J. Cho, *Nat. Commun.* **2017**, *8*, 812.

[17] A. G. Tamirat, Y. Lui, X. L. Dong, C. X. Wang, Y. G. Wang, Y. Y. Xia, *Small Struct.* **2021**, *2*, 2000126.

[18] S. B. Tu, X. Ai, X. C. Wang, S. W. Gui, Z. Cai, R. M. Zhan, Y. C. Tan, W. W. Liu, H. Yang, C. H. Li, Y. M. Sun, *J. Energy Chem*. **2021**, *62*, 477.

[19] J. Sun, H.-W. Lee, M. Pasta, H. T. Yuan, G. Y. Zheng, Y. M. Sun, Y. Z. Li, Y. Cui, *Nat. Nanotech.* **2015**, *10*, 980.

[20] Y. M. Sun, L. Wang, Y. B. Li, Y. Z. Li, H. R. Lee, A. Pei, X. M. He, Y. Cui, *Joule* **2019**, *3*, 1.

[21] H. C. Jin, S. Xin, C. H. Chuang, W. D. Li, H. Y. Wang, J. Zhu, H. Y. Xie, T. M. Zhang, Y. Y. Wan, Z. K. Qi, W. S. Yan, Y.-R. Lu, T.-S. Chan, X. J. Wu, J. B. Goodenough, H. X. Ji, X. F. Duan, *Science* **2020**, *370*, 192.

[22] R. Y. Tian, S.-H. Park, P. J. King, G. Cunningham, J. Coelho, V. Nicolosi, J. N. Coleman, *Nat. Commun.* **2019**, *10*, 1933.

[23] J. Billaud, F. Bouville, T. Magrini, C. Villevieille, A. R. Studart, *Nat. Energy* **2016**, *1*, 16097.

[24] K.-H. Chen, V. Goel, M. J. Namkoong, M. Wied, S. Müller, V. Wood, J. Sakamoto, K. Thornton, N. P. Dasgupta, *Adv. Energy Mater.* **2021**, *11*, 200336.

[25] J. Sander, R. Erb, L. Li, A. Gurijala, Y.-M. Chiang, *Nat. Energy* **2016**, *1*, 16099.

[26] Y. Liu, Y. Zhu, Y. Cui, *Nat. Energy* **2019**, *4*, 540.

[27] X.-D. Zhang, F.-S. Yue, J.-Y. Liang, J.-L. Shi, H. Li, Y.-G. Guo, *Small Struct.* **2020**, *1*, 2000042.

[28] L. Shen, S. Chen, J. Maier, Y. Yu, *Adv. Mater.* **2017**, *29*, 1701571.

[29] N. Liu, Z. D. Lu, J. Zhao, M. T. McDowell, H.-W. Lee, W. T. Zhao, Y. Cui, *Nat. Nanotech.* **2014**, *9*, 187.

[30] L. Wang, J. W. Wan, J. Y. Wang, D. Wang, *Small Struct.* **2021**, *2*, 2000041.

[31] F. X. Wu, V. Srot, S. Q. Chen, S. Lorger, P. A. van Aken, J. Maier, Y. Yu, *Adv. Mater.* **2019**, *31*, 1905146.

[32] A. Adam, J. Wandt, E. Knobbe, G. Bauer, A. Kwade, *J. Electrochem. Soc.* **2020**, *167*, 130503.

[33] X. X. Jiao, Y. Y. Liu, T. T. Li, C. F. Zhang, X. Y. Xu, O. O. Kapitanova, C. He, B. Li, S. Z. Xiong, J. X. Song, *ACS Appl. Mater. Interfaces* **2019**, *11*, 30858.

[34] X. Zhang, Z. Y. Ju, L. M. Housel, L. Wang, Y. Zhu, G. Singh, N. Sadique, K. J. Takeuchi, E. S. Takeuchi, A. C. Marschilok, G. H. Yu, *Nano Lett.* **2019**, *19*, 8255.

[35] H. T. Sun, L. Mei, J. F. Liang, Z. P. Zhao, C. Lee, H. L. Fei, M. N. Ding, J. Lau, M. Li, C. Wang, X. Xu, G. L. Hao, B. Papandrea, I. Shakir, B. Dunn, Y. Huang, X. F. Duan, *Science* **2017**, *356*, 599.

[36] Y. Z. Shi, B. Li, Y. Z. Zhang, Y. Cui, Z. J. Cao, Z. G. Du, J. N. Gu, K. Shen, S. B. Yang, *Adv. Energy Mater.* **2021**, *11*, 2003663.

[37] C. J. Chen, Y. Zhang, Y. J. Li, Y. D. Kuang, J. W. Song, W. Luo, Y. B. Wang, Y. G. Yao, G. Pastel, J. Xie, L. B. Hu, *Adv. Energy Mater.* **2017**, *7*, 1700595.

[38] Y, Zhang, W. Luo, C. W. Wang, Y. J. Li, C. J. Chen, J. W. Song, J. Q. Dai, E. M. Hitz, S. M. Xu, C. P. Yang, Y. B. Wang, L. B. Hu. *Proc. Natl. Acad. Sci. USA* **2017**, *114*, 3584.

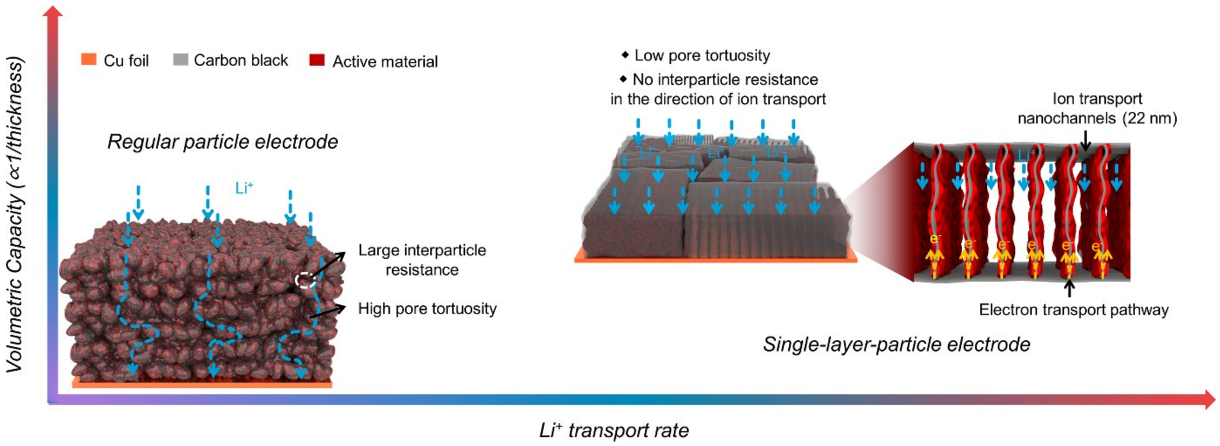

Figure 1. Schematic illustration of regular particle electrode consisting of randomly stacked active particles with high tortuosity and single-layer chunky particle electrode with low-tortuosity inner nanochannels for ion transport and conductive pathway for electron transfer. Active particles with random charge transport orientations are randomly stacked in traditional electrodes, which leads to high tortuosity and inner particle/electrode resistance. Vertical inner nanochannels enable fast ion transport and conducting pathways accelerate electron transport in single-layer chunky particle electrode.

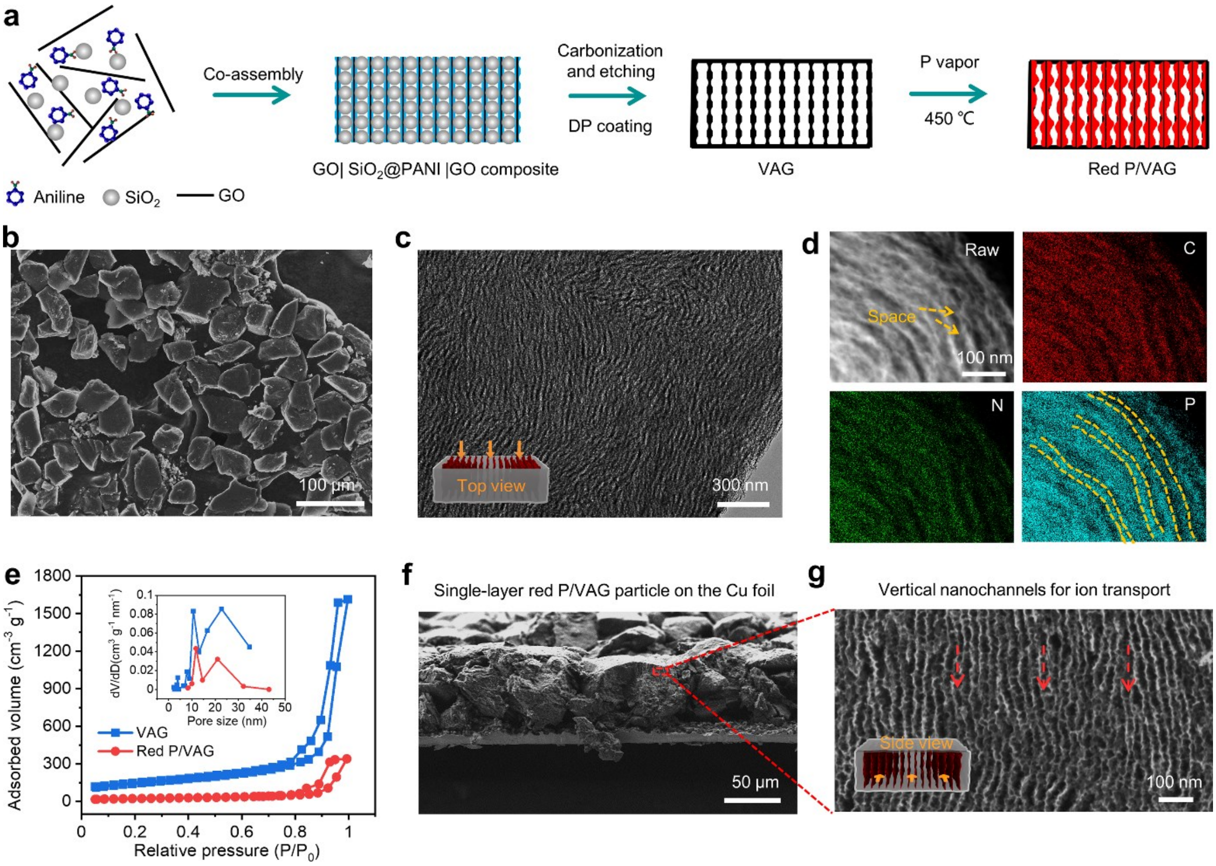

Figure 2. (a) Schematic illustration of the fabrication of red P/VAG composite. (b and c) SEM (b) and TEM (c) images of VAG. (d) Dark-field STEM and corresponding elemental mapping images of red P/VAG composite. (e) Nitrogen adsorption/desorption isotherms of VAG and red P/VAG composite. (f and g) Cross-section SEM images of single-layer red P/VAG particle electrode. The inset in (e) showed pore size distribution plots of VAG and red P/VAG composite.

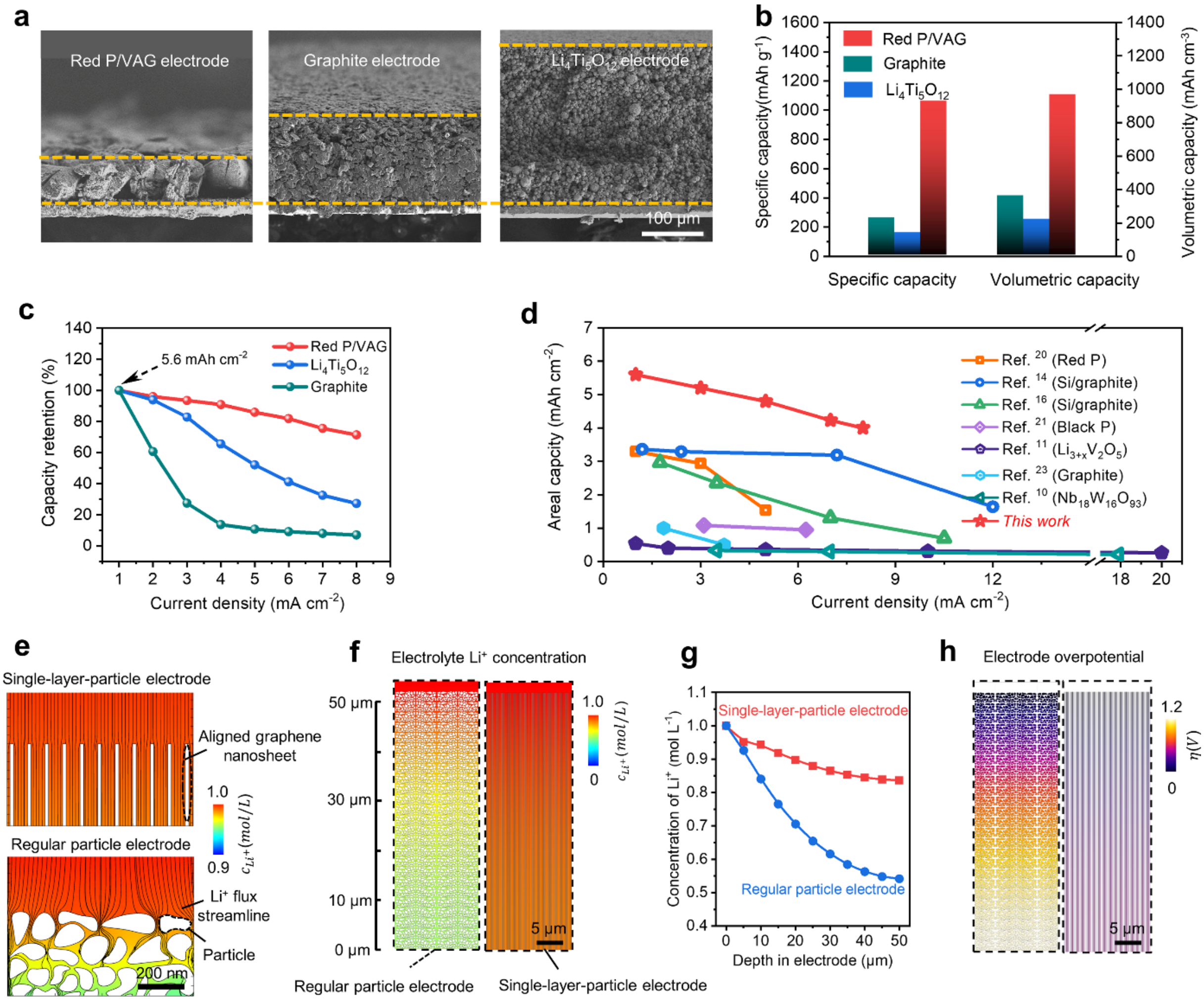

Figure 3. (a-c) Cross-section SEM images (a), the comparison of the capacities based on the total weight and volume of the single-layer red P/VAG particle electrode and commercial graphite and $Li_4Ti_5O_{12}$ electrodes with the same areal capacity of ~ 5.6 mAh cm^{-2} (b), the comparison of capacity retentions for single-layer red P/VAG, commercial $Li_4Ti_5O_{12}$ and graphite electrodes at various current densities (c). The volumetric capacities of all electrodes were calculated based on their thickness before

cycling. (d) Comparison of the rate capability between single-layer red P/VAG particle electrode and other reported fast-charging anodes. Zoom out of Li⁺ flux in the electrolyte in the vicinity of single-layer chunky particle and regular particle electrode/electrolyte interfaces (e-h). Li⁺ concentration in electrolyte *vs*. depth in electrode plots (e, f) in two electrodes, Li⁺ concentration distribution in electrolyte (g) and electrode overpotentials (h).

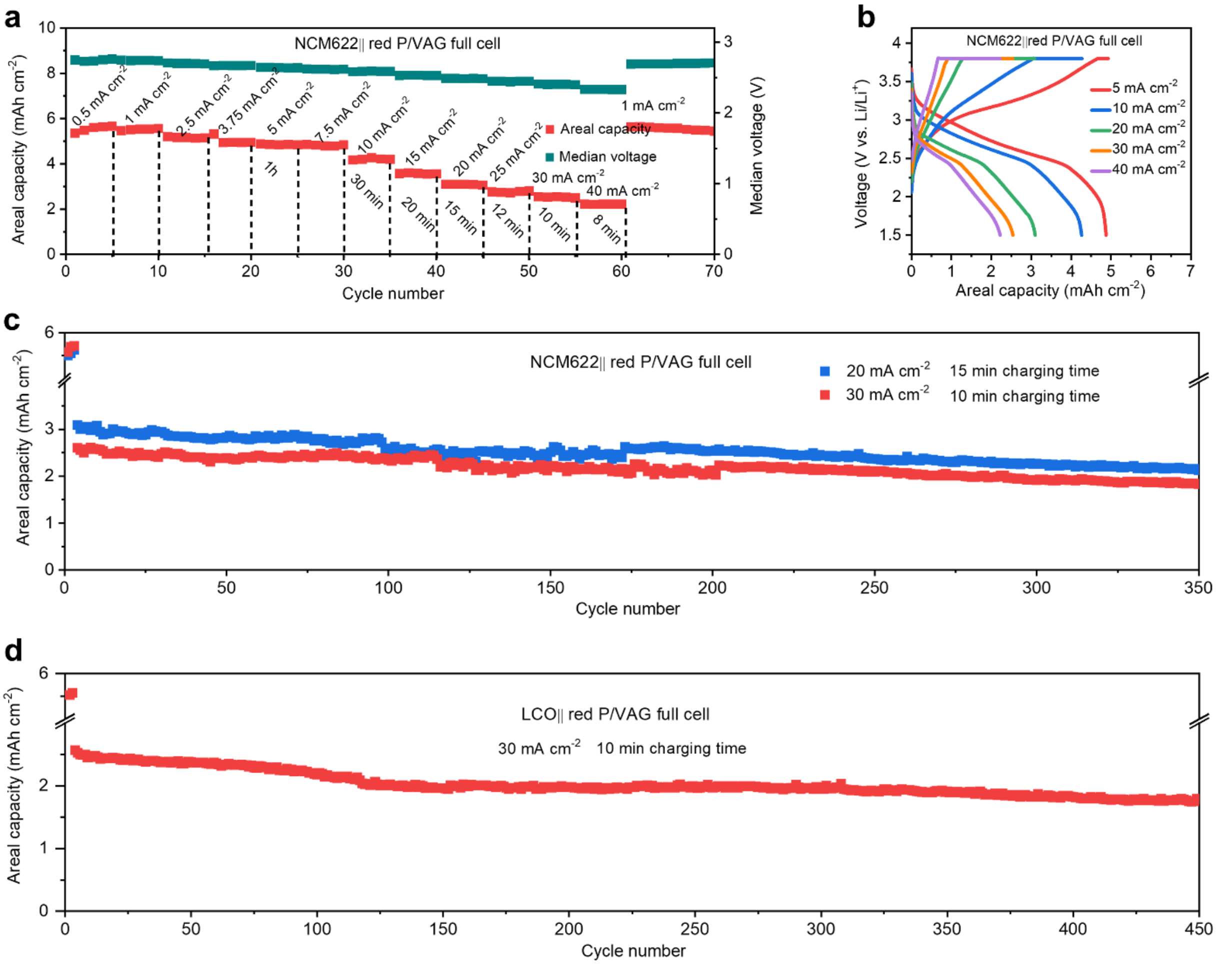

Figure 4. (a and b) Rate capability and median voltages (a), and voltage profiles (b) of NCM622||single-layer red P/VAG full cell at various charging current densities from 1 to 40 mA cm^{-2}. The charging times were 60, 30, 20, 15, 12, 10 and 8 min at 5, 10, 15, 20, 25, 30 and 40 mA cm^{-2}, respectively. (c and d) Cycling stability of NCM622||single-layer red P/VAG full cell at 20 and 30 mA cm^{-2} (d), and LCO||single-layer red P/VAG full cell at 30 mA cm^{-2} (d).

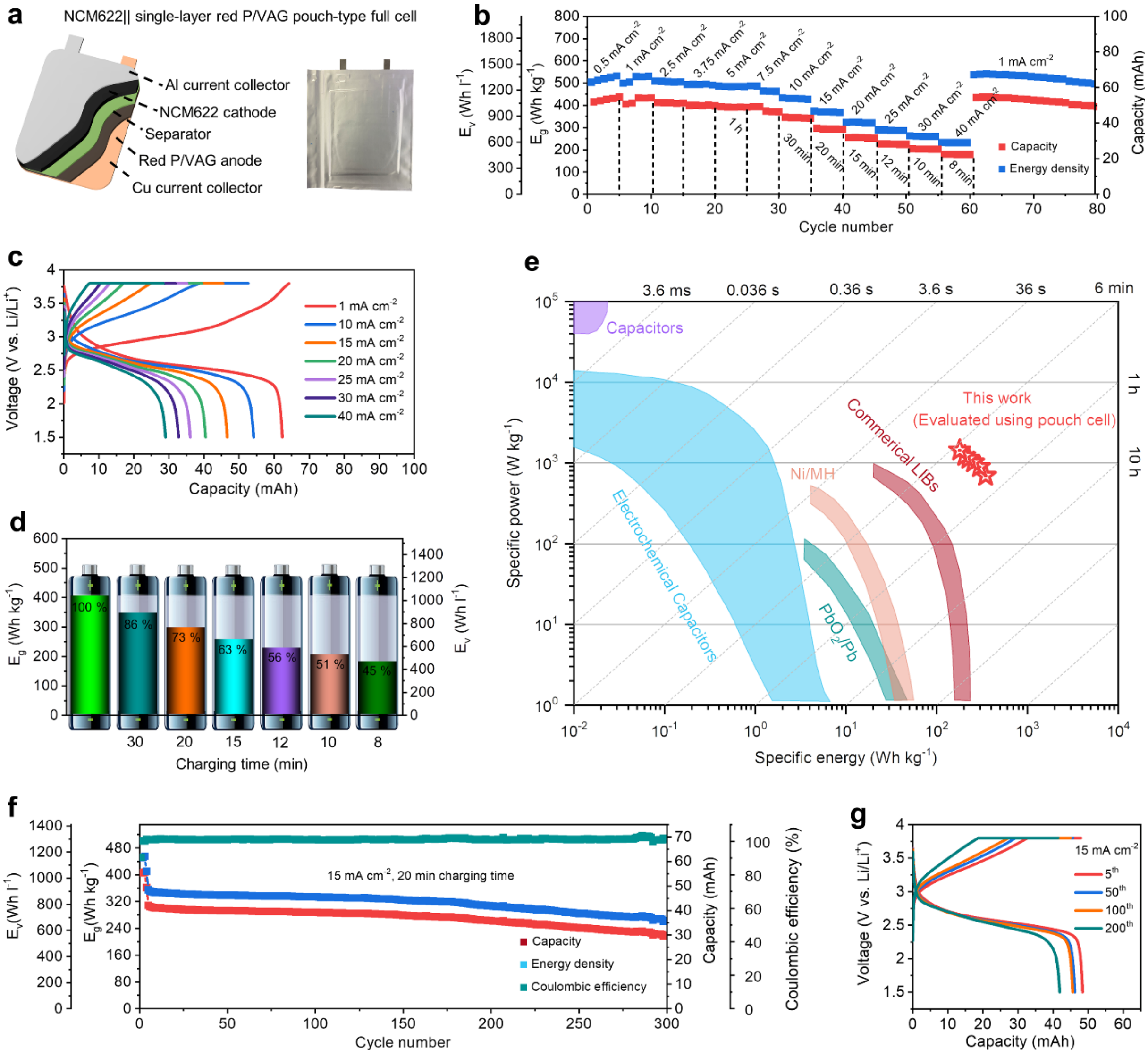

Figure 5. (a) The pouch cell configuration using single-layer red P/VAG particle electrode. (b and c) Rate capability (b) and charge/discharge profiles (c) of NCM622||single-layer red P/VAG pouch cell at various charging current densities from 1 to 40 mA cm^{-2}. The discharge current density was fixed as 0.5 mA cm^{-2}. (d) E_g and E_v achieved within the charging times of 30, 20, 15, 12, 10 and 8 min. (e) Ragone

(double logarithmic) plots of energy density and power density for electrochemical energy storage devices and NCM622||single-layer red P/VAG full cell based on the pouch cell data. (f) The cycling performance of NCM622||single-layer red P/VAG pouch cell at the high charging current density of 15 mA cm^{-2} (corresponding to the charge time of 20 minutes) and (g) charge/discharge profiles for different cycles. The pouch cell was activated at 0.5 mA cm^{-2} for three cycles.

Declaration of interests

The authors declare no competing financial interest.

Supporting Information

Supporting Information is available from the Wiley Online Library or from the author.

Acknowledgments

This work is financially supported by the Natural Science Foundation of China (Grant No. 520721137) and the Innovation Fund of Wuhan National Laboratory for Optoelectronics of Huazhong University of Science and Technology. The authors would like to thank the Analytical and Testing Center of Huazhong University of Science and Technology (HUST) as well as the Center for Nanoscale Characterization & Devices of Wuhan National Laboratory for Optoelectronics (WNLO) for providing the facilities to conduct the characterizations. The authors also thank Shiyanjia Lab (www.shiyanjia.com) for the porous structure measurement. Z.W.S. acknowledges the support of the Singapore National Research Foundation (NRF-

NRFF2017-04) and Agency for Science, Technology and Research (Central Research Fund Award).

Received: ((will be filled in by the editorial staff))

Revised: ((will be filled in by the editorial staff))

A single-layer chunky particle electrode with vertically aligned charge transport pathways was designed, which addressed the slow charge transport issue of common high-areal-capacity electrodes caused by their high tortuosity and interparticle resistance, and simultaneously realized the fast-charging capability and high energy density of Li-ion batteries.

Keywords: single-layer-particle electrode, fast charging, high power density, high energy density, red phosphorus

Shuibin Tu, Ziheng Lu, Mengting Zheng, Zihe Chen, Xiancheng Wang, Zhao Cai, Chaoji Chen, Li Wang, Chenhui Li, Zhi Wei Seh, Shangqing Zhang, Jun Lu*, and Yongming Sun*

Single-Layer-Particle Electrode Design for Practical Fast-Charging Lithium-ion Batteries

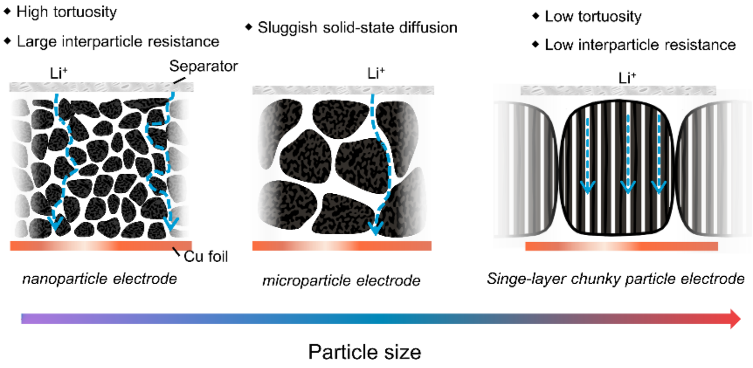
◆ High tortuosity
◆ Large interparticle resistance
◆ Sluggish solid-state diffusion
◆ Low tortuosity
◆ Low interparticle resistance
Li⁺
Separator
Li⁺
Li⁺
Cu foil
nanoparticle electrode
microparticle electrode
Singe-layer chunky particle electrode
Particle size